Volume extreme ultraviolet holographic imaging with numerical optical sectioning

P. W. Wachulak, M. C. Marconi, R. A. Bartels, C. S. Menoni, and J. J. Rocca

NSF ERC for Extreme Ultraviolet Science & Technology and Department of Electrical and Computer Engineering, Colorado State University, USA

Abstract: Three dimensional images were obtained using a single high numerical aperture hologram recorded in a high resolution photoresist with a table top λ = 46.9 nm laser. Gabor holograms were numerically reconstructed over a range of image planes by sweeping the propagation distance in the numerical reconstruction algorithm, allowing numerical optical sectioning. A robust three dimension image of a test object was obtained with numerical optical sectioning, providing a longitudinal resolution of approximately 2 μm and a lateral resolution of 164 nm.

©2007 Optical Society of America

OCIS codes: (090.0090) Holography; (100.2960) Image analysis

References and Links

1. J. E. Trebes, S. B. Brown, E. M. Campbell, D. L. Matthews, D. G. Nilson, G. F. Stone, and D. A. Whelan, "Demonstration of X-Ray holography with an X-Ray laser," Science **238**, 517-519 (1987).
2. S. Lindaas, M. Howells, C. Jacobsen and A. Kalinovsky. "X-ray holographic microscopy by means of photoresist recording and atomic force microscope readout," J. Opt. Soc. Am. A **13**, 1788-1800 (1996).
3. I. McNulty, J. Kirz, C. Jacobsen, E. Anderson, M. R. Howells, and D. P. Kern, "High resolution imaging by Fourier Transform X-ray holography," Science **256**, 1009-1012 (1992).
4. C. Jacobsen, M. Howells, J. Kirz, and S. Rothman, "X-ray holographic microscopy using photoresist," J. Opt. Soc. Am. A **7**, 1847-1861 (1990).
5. I. McNulty, "The future of X-ray holography," Nucl. Instrum. Methods Phys. Res. A **347**, 170-176 (1994).
6. S. Eisebitt, J. Lüning, W. F. Schlotter, M. Lörgen, O. Hellwing, W. Eberhardt and J. Stöhr, "Lensless imaging of magnetic nanostructures by X-ray spectro-holography," Nature **432**, 885-888 (2004).
7. R. A. Bartels, A. Paul, H. Green, H. C. Kapteyn, M. M. Murnane, S. Backus, I. P. Christov, Y. W. Liu, D. Attwood, and C. Jacobsen. "Generation of spatially coherent light at extreme ultraviolet wavelengths," Science **297**, 376-378 (2002).
8. A. S. Morlens, J. Gautier, G. Rey, P. Zeitoun, J. P. Caumes, M. Kos-Rosset, H. Merdji, S. Kazamias, K. Cassou and M. Fajardo, "Submicrometer digital in-line holographic microscopy at 32 nm with high-order harmonics," Opt. Lett. **31**, 3095-3097 (2006).
9. R. I. Tobey, M. E. Siemens, O. Cohen, M. M. Murnane, H. C. Kapteyn and K. A. Nelson, "Ultrafast extreme ultraviolet holography: dynamic monitoring of surface deformation," Opt. Lett. **32**, 286-288 (2007).
10. C. D. Macchietto, B. R. Benware and J. J. Rocca, "Generation of millijoule-level soft-X ray laser pulses at a 4-Hz repetition rate in a highly saturated tabletop capillary discharge amplifier," Opt. Lett. **24**, 1115-1117 (1999).
11. Y. Wang, M. A. Larotonda, B. M. Luther, D. Alessi, M. Berrill, V. N. Shlyaptsev, and J. J. Rocca, "Demonstration of high-repetition-rate tabletop soft-x-ray lasers with saturated output at wavelengths down to 13.9 nm and gain down to 10.9 nm," Phys. Rev. A **72** Art. No. 053807 (2005).
12. G. Vaschenko, C. Brewer, F. Brizuela, Y. Wang, M. A. Larotonda, B. M. Luther, M. C. Marconi, J. J. Rocca, C. S. Menoni, E. H. Anderson, W. Chao, B. D. Harteneck, J. A. Liddle, Y. Liu, D. T. Attwood. "Sub-38 nm resolution table-top microscopy using 13 nm wavelength laser light," Opt. Lett. **31**, 1214-1216 (2006).
13. G. Vaschenko, F. Brizuela, C. Brewer, M. Grisham, H. Mancini, C. S. Menoni, M. C. Marconi, J. J. Rocca, W. Chao, A. Liddle, E. Anderson, D. Attwood, A. V. Vinogradov, I. A. Artioukov, Y. P. Pershyn and V. V. Kondratenko. "Nano-imaging with a compact extreme ultraviolet laser," Opt. Lett. **30**, 2095-2097 (2005).
14. F. Brizuela, G. Vaschenko, C. Brewer, M. Grisham, C. S. Menoni, M. C. Marconi, J. J. Rocca, W. Chao, J. A. Liddle, E. H. Anderson, D. T. Attwood, A. V. Vinogradov, I. A. Artiukov, Y. P. Pershing and V. V. Kondratenko, "Reflection Mode Imaging with Nanoscale Resolution using a Compact Extreme Ultraviolet Laser," Opt. Express **13**, 3983-3988 (2005).
15. B. R. Benware, C. D. Macchietto, C. H. Moreno, and J. J. Rocca, "Demonstration of a high average power tabletop soft X-ray laser," Phys. Rev. Lett. **81**, 5804-5807 (1998).
16. J. J. Rocca, "Table-top soft x-ray lasers," Rev. Sci. Instrum. **70**, 3799-3827 (1999).

17. J. J. Rocca, D. P. Clark, J. L. A. Chilla, V. N. Shlyaptsev, "Energy extraction and achievement of the saturation limit in a discharge-pumped table-top soft x-ray amplifier," Phys. Rev. Lett. **77**, 1476-1479 (1996).
18. P. W. Wachulak, R. A. Bartels, M. C. Marconi, C. S. Menoni and J. J. Rocca. "Sub-400 nm spatial resolution extreme ultraviolet holography with table top laser," Opt. Express **14**, 9636-9642 (2006).
19. Center for X-Ray Optics. http://www-cxro.lbl.gov.
20. Suspension 2.62% in water of latex spheres from Polysciences Inc., diameter 465 nm.
21. U. Schnars and P. O. Jüptner, "Digital recording and reconstruction of holograms in hologram interferometry and shearography," Appl. Opt. **33**, 4373-4377 (1994).
22. U. Schnars and P. O. Jüptner, "Digital recording and numerical reconstruction of holograms," Meas. Sci. Technol. **13**, R85-R101 (2002).
23. J. W. Goodman, *Introduction to Fourier Optics* (McGraw Hill, 1996), Chap 4, p. 66.
24. G. L. Rogers. "Gabor diffraction microscopy. The hologram as a generalized zone-plate," Nature **166**, 236-237 (1950).
25. Attwood, *Soft X-ray and extreme ultraviolet radiation*, (Cambridge University Press. 1999), Chap. 9, p. 361.

1. Introduction

Holographic imaging in the soft X-ray (SXR) and extreme ultraviolet (EUV) spectral region has been demonstrated with EUV/SXR lasers, high harmonic generation (HHG), and synchrotron sources. These include the first realization of SXR laser holography at Lawrence Livermore National Laboratory using a large laser facility, and the holographic recording of biological samples and sub-micron structures using SXR radiation at synchrotron facilities, among other experiments. [1-3] Using synchrotron radiation Gabor and Fourier holograms have been demonstrated with spatial resolution below 100 nm at SXR wavelengths [4-6].

Compact EUV sources based on high harmonic generation (HHG) have produced table-top EUV Gabor holographic images with spatial resolutions of 7.9 µm [7] and 0.8 µm [8]. Time resolved holographic imaging, that exploits the short pulsewidth of the HHG sources, was also implemented to study the ultrafast dynamics of surface deformation with a lateral resolution of the order of 100 nm [9]. The recent development of compact coherent EUV laser sources [10, 11] has opened new opportunities for the implementation of novel imaging schemes with sub-micron spatial resolution that fit on a table-top [12-14].

In this paper, we present a proof of principle experiment in which we demonstrate that three dimensional imaging in a volume may be obtained from a single high numerical aperture (NA) hologram. The three dimensional images were obtained with Gabor holograms recoded in photoresist after exposure by a table-top EUV laser. Digitized holograms were numerically reconstructed over a range of image planes by numerically sweeping the reconstruction distance, resulting in numerical optical sectioning of image depths.

2. Experimental details

The experimental set up is schematically illustrated in Fig. 1. A compact $\lambda=46.9$ nm table top discharge-pumped capillary Ne-like Ar laser occupying only a 1×0.5 m^2 footprint on an optical table was used for recording the hologram. Lasing was obtained in the 46.9 nm 3s $^1P_1$ – 3p $^1S_0$ transition of neon-like Ar after exciting Ar filled alumina capillaries 3.2 mm in diameter with a current pulse having an amplitude of $\approx$ 24 kA, a 10% to 90% rise time of $\approx$25 ns and a first half-cycle duration of $\approx$110 ns [10,15]. The fast current pulse was produced by discharging a water dielectric cylindrical capacitor through a spark gap switch connected in series with the capillary load. The current pulse rapidly compresses the plasma column to achieve a dense and hot filamentary plasma channel where a population inversion is created by strong monopole electron impact excitation of the laser upper level and rapid radiative relaxation of the laser lower level [16, 17]. The water serves as a liquid dielectric for the capacitor and also cools the capillary. A continuous flow of Ar is injected in the front of the capillary
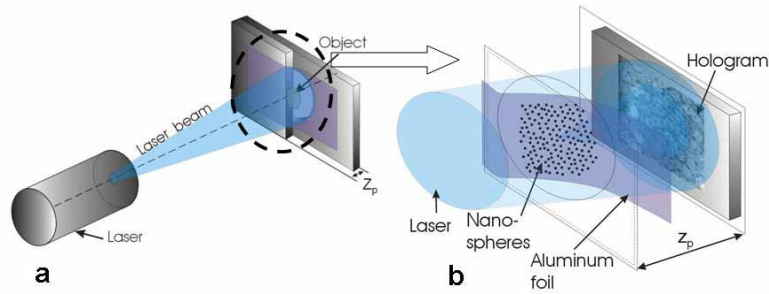
Fig. 1. (a). Diagram of the experimental set up. b) Detail of the test object used.

and an optimum Ar gas pressure of 490 mTorr is maintained in the capillary channel. The EUV laser and the vacuum chamber where the hologram was exposed are connected via a vacuum manifold that provides differential pumping of the chamber that is maintained at $\sim 10^{-5}$ Torr. The laser operated with 18.4 cm long capillaries produces 0.1 mJ pulses at a repetition rate of 1 Hz [15]. The high temporal and spatial coherence of the EUV table top laser permits the recording of large NA holograms for high resolution holographic imaging [18].

The test object used in the holographic volume imaging experiment consisted of a tilted metallic surface covered with opaque spherical markers. This test object was fabricated placing a 100 nm thick aluminum foil covering a hole 1.5 mm in diameter made in a 80 µm thick Mylar sheet. The hole was partially covered with a second Mylar sheet 80 µm thick, as schematically indicated in Fig. 1(b). The aluminum foil contours over the semicircular aperture to produce a variable height surface with the desirable characteristics for this test. The 100 nm aluminum foil has a transmission of approximately 35% at λ=46.9 nm limited mainly by a layer of native oxide [19]. The Al filter also suppresses the lower photon energy plasma emission (i.e., long wavelength background) from the Ar discharge in the laser source.

The object was prepared by placing a drop of water with a suspension of latex spheres, 465 nm in diameter [20] on the aluminum foil membrane. Evaporation of the water left a random distribution of latex spheres deposited over the partially transparent tilted Al foil membrane. Note that these spheres are completely opaque to the 46.9 nm EUV laser radiation. With this deposition procedure, these markers are distributed at locations yielding a range of distances from the photoresist where the holograms are subsequently recorded.

The holograms were recorded by exposing a 120 nm thick layer of PMMA (MicroChem 950,000 molecular weight) spin-coated on a silicon wafer to the Gabor hologram interference pattern produced by the illuminating EUV laser beam. To activate PMMA with 46.9 nm radiation requires exposures in the range of $\sim 2\times10^7$ photons µm^{-2}. Given the laser parameters quoted above, such exposure levels require approximately 240 laser shots, equivalent to a 4 minutes exposure time at the repetition rate employed in this experiment. After exposure, the photoresist was developed using standard development procedures. The hologram was immersed in a solution of MIBK-methyl isobutyl ketone (4-Methyl-2-Pentanone) with IPA (isopropyl alcohol) 1:3 for 30 seconds, rinsed with IPA for 30 seconds, and dried with nitrogen.
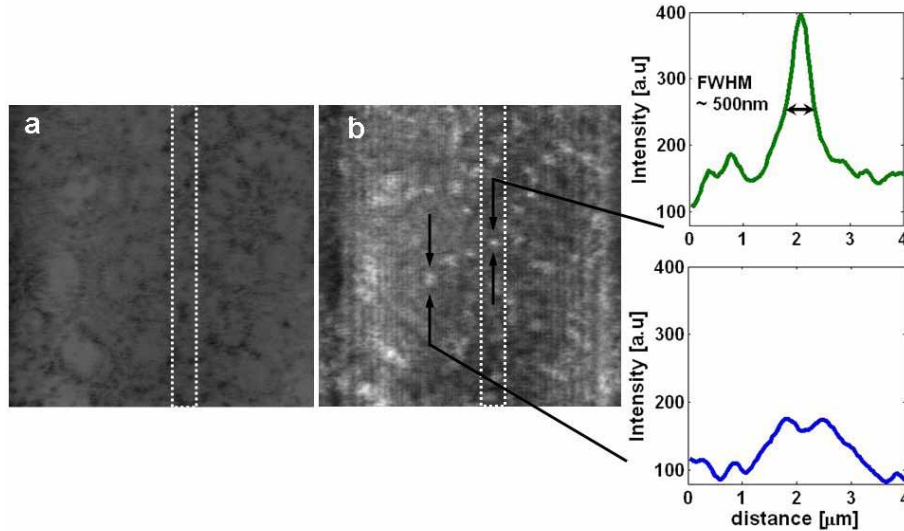
Fig. 2. (a). Hologram of the sample with a random distribution of 465nm diameter latex spheres over the tilted surface of an Al foil recorded in the photoresist surface and digitized with an atomic force microscope. b) Digital reconstruction of the hologram. Right: intensity cuts in the vertical direction of one "in focus" marker (top curve) and one "out of focus" marker (bottom curve). The white dotted lines indicate the region in the reconstruction that is "in focus".

3. Results

During the recording phase of the Gabor holography, we carefully adjusted the exposure so that the photoresist operated in a linear response regime. After exposure by the EUV laser, the holographic interference pattern generated by the reference and the object beams was recorded in the photoresist and converted to a surface modulation after the development. Thus, the holograms were recorded as a relief pattern in the surface of a photoresist deposited on a Si wafer. Holograms recorded in such a fashion can not be reconstructed in the conventional way with an optical reconstruction beam. In order to numerically reconstruct the holograms, the surface modulation was digitized with a Novascan atomic force microscope (AFM) operated in "tapping" mode. Two holograms digitized in this manner are displayed in Fig. 2(a) and Fig. 5(a).

The digital reconstruction of the hologram digitized by the AFM is based on a numerical Fresnel propagator [21-23]. To obtain the amplitude and the phase distribution of the field in the image plane, the simulated field emerging from the hologram illuminated by a plane wave is numerically back propagated with the Fresnel-Kirchhoff integral. The integral was evaluated by the product of the spatial frequency representation of the hologram obtained through a two dimensional fast Fourier transformation and the quadratic phase free space Fresnel propagator in the spatial frequency domain. The back-propagation distance is determined by calculating the Fresnel zone plate (FZP) focal distance for the specific hologram geometry [7]. For the specific geometry employed in this experiment, the FZP focal length is approximately the distance between the object and the recording medium. The digital images of the holograms processed with the Fresnel propagation code generated the reconstructed images shown in Fig. 2(b) and Fig. 5(b).

Figure 2(a) shows a small section of the hologram with an area $42 \times 42 \ \mu m^2$. The numerical reconstruction of the hologram using a Fresnel propagator provided images of the object described above and schematically shown in Fig. 1(b). One of the critical parameters in the

reconstruction code is the distance between the recording medium and the object, indicated in the diagram of Fig. 1 as z_p. Small changes in z_p reconstructs slightly different images. To determine the value of z_p corresponding to the optimum reconstruction, an image correlation technique was utilized as described in detail in reference 18. The images reconstructed for different z_p were correlated with a set of synthesized images with decreasing resolution. This set of decreasing resolution images (wavelet components) were obtained by wavelet decomposition from a reference image constructed to have 1 pixel resolution. Each wavelet component has a relative resolution to the reference image $Y = 2^X$, where Y is the relative resolution between the reference and the wavelet component and X is the scale of the wavelet. The z_p for the best reconstruction was determined by maximizing the value of the correlation between the reconstructed image and the wavelet components.

To demonstrate the retrieval of the depth information from the hologram we ran the reconstruction code with the digitized image of the hologram shown in Fig. 2(a) for different values of the distance z_p. The different runs produced different reconstructed images in which the latex spheres markers located at the correct z_p generated a sharper image than those markers "out of focus". Figure 2(b) shows one of these reconstructed images. In this case the reconstruction is optimum for a distance z_p that matches the height of the central part of the hologram, indicated in the figure by two white dotted lines. In this strip the height is such that the markers located in this region reconstruct "in focus", while the latex spheres above and below this level are reconstructed blurred. This can be observed in Fig. 2 (right) where the intensity profiles obtained in a vertical cut of one "in focus" marker (top) and one "out of focus" marker (bottom) are plotted. By changing z_p in the reconstruction code only the latex sphere markers located at a height equal to z_p produced sharper images as compared to those markers out of focus. This is a similar effect to optical sectioning but performed on a digitally reconstructed image.

The depth information in the hologram can finally be retrieved varying the reconstruction parameter z_p. To determine the value of z_p at which the best reconstruction is obtained we correlated the reconstructed image with a template of the marker consisting of a circular mask with the size of the latex sphere. Finding the maximum value of the correlation between the reconstructed image of each marker and the mask determines the corresponding optimum height. Combining this information with the *x-y* coordinates of each marker allowed for a complete determination of the marker position and a reconstruction of the surface of the test object with depth resolution. Figures 3(a) and 3(b) show the surface topography obtained from the reconstructed images in two different regions of the hologram. In the case of Fig. 3(a), the AFM scan was performed in a region of the test object close to the edge of the Mylard spacer, where the slope of the aluminum foil is expected to be high. A similar scan performed at a distance approximately 200 μm away from this edge, produced an image with smaller slope as shown in Fig. 3(b).
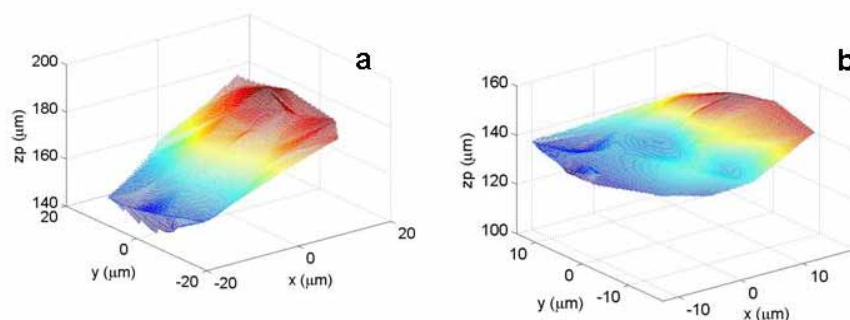

Fig. 3. Surface topographies obtained from reconstructed images in different regions of the object. a) Region close to the edge of the spacer where a high slope is revealed, b) Region approximately 200 μm away from the edge showing a lower slope.
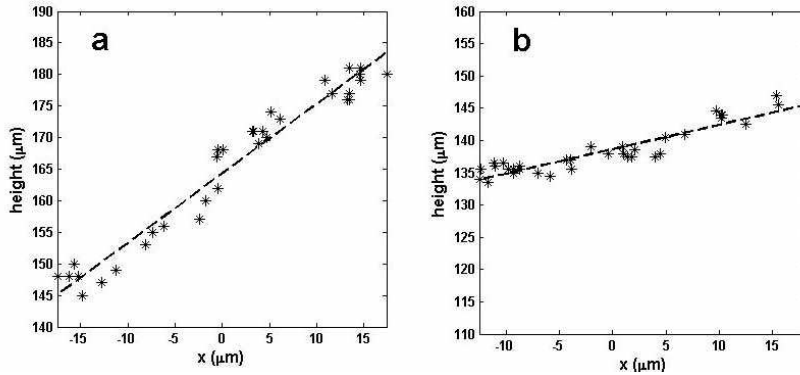
Fig. 4. Calculated heights of the markers in two different positions of the object. a) Close to the edge of the Maylard spacer where a higher slope is expected. b) Approximately at 200 μm from the edge, where a smaller slope was measured. These two plots correspond to the same regions plotted in Fig. 3(a) and Fig. 3(b) respectively.

Figure 4 shows the calculated heights for all markers as a function of the transversal coordinate x in the same two regions of the object plotted in Fig. 3. In the plots shown in Fig. 4, all markers are represented regardless of its y coordinate. These plots give a measure of the spread of the calculated heights for all the markers and also show, as indicated by the best linear fit, the different slopes in the two regions. The statistical dispersion of the data points relative to the best linear fit are $\Delta z = 2.64$ μm for the region with high slope (Fig. 4(a)) and $\Delta z = 1.32$ μm for the region with lower slope (Fig. 4(b)). This spread in the measured heights of the markers compares well with the expected accuracy in the z direction determined by the NA utilized recording the hologram. As pointed out by Rogers, if one assumes the hologram as a superposition of FZPs [24], the resolution in the z coordinate can be related to its depth of focus. For a FZP the depth of focus is given by $\delta z = \lambda / NA^2$. [25] The NA corresponding to the higher slope region where $z_p = 160$ μm is NA = 0.13, yielding a depth of focus $\delta z = 2.77$ μm. In the region where the Al foil has a lower slope, the latex markers were closer to the hologram, at a distance $z_p = 140$ μm. For this reconstruction the expected vertical resolution is $\delta z = 2.12$ μm.

The lateral resolution of the reconstructed images is also determined by the NA of the recording. In the test object, as the distance from the markers to the photoresist changes across the hologram, so varies the NA and the lateral resolution. To assure that the markers were well resolved in the lateral direction we performed an auxiliary experiment with a second hologram of a broken AFM tip, shown in Fig. 5(a). The NA in this auxiliary experiment was
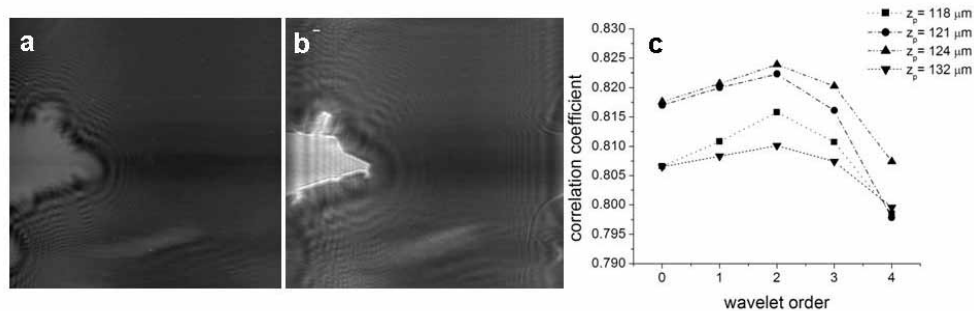

Fig. 5. (a). Small section (42×42 μm^2) of the hologram of a broken AFM tip recorded in the surface of PMMA photoresist. (b). Optimum reconstruction of the hologram depicted in a). c) Correlation curves showing that the reconstruction is optimum for the wavelet order 2 for a wide range of z_p indicating a lateral resolution of $2^2 = 4$ pixels, for this case $\Delta = 164$ nm.

similar to the NA used in the recording of the hologram of the test object in the first experiment. Figure 5(b) is the best reconstruction obtained by image correlation with a set of lower resolution wavelet components, in a similar way as described in Ref [18]. Figure 5(c) is the plot of the correlation values for different images reconstructed with different object-hologram distances and different wavelet components as a function of the wavelet scale X. The figure shows a maximum in the correlations for X = 2 at all reconstruction distances ranging from z_p=116 μm to z_p=132 μm, thus setting the spatial resolution to $2^2 = 4$ pixels. In the reconstruction shown in Fig. 5(b), the pixel size corresponds to 41 nm. This indicates that the spatial resolution in the image is Δ=164 nm. This value also compares very well with the expected resolution based on the Rayleigh criterion, Δ= (0.61 λ)/NA, which for this set up is 166 nm.

4. Conclusions

We have demonstrated that through detailed processing of the reconstructed holographic images, performed by changing the object-hologram distance in the reconstruction code, it is possible to discriminate depth in the object. Using a specially fabricated object composed of spherical markers 465 nm in diameter spread on a tilted transparent surface, the reconstruction and analysis of the hologram allowed to map the surface topography with a resolution close to 2 μm, with such resolution depending on the particular NA of the exposure. The lateral resolution of the image obtained by numerical reconstruction was assessed utilizing a wavelet image decomposition and image correlation. The best lateral resolution obtained with a high NA recording, 164 nm, represents an improvement of more than a factor two relative to previously published results.

Acknowledgments